Journal of Information Technology and Cyber Security 3(2) July 2025: 128-146 EISSN 2987-386X | PISSN 2987-3878
DOI: 10.30996/jitcs.132037

Research Article | Mufti & Whardana

Early Breast Cancer Detection Using Gabor Filter and Convolutional Neural Network for Microcalcification Identification

Abdul Latief Mufti [1,*] and Adithya Kusuma Whardana [2,]

[1,2] Department of Informatics Engineering, Universitas Tanri Abeng, Indonesia
* Corresponding author: abdul.latief@student.tau.ac.id

Received: 23 May 2025
Accepted: 15 September 2025
Revised: 8 September 2025
Available online: 07 October 2025

To cite this article: Mufti, A. L., & Whardana, A. K. (2025). Early Breast Cancer Detection Using Gabor Filter and Convolutional Neural Network for Microcalcification Identification. *Journal of Information Technology and Cyber Security, 3*(2), 128-146. https://doi.org/10.30996/jitcs.132037

Abstract

Breast cancer poses a considerable challenge in Indonesia, resulting in numerous fatalities. This study aims to improve the accuracy and efficiency of early breast cancer diagnosis by leveraging modern image processing and artificial intelligence. The dataset used is the Mini-DDSM (Mini Digital Database for Screening Mammography), taken from Kaggle and vetted by radiologists into a Region of Interest (ROI) consisting of three categories: Benign, Cancer, and Normal. The methodology encompasses comprehensive image preprocessing, which includes resizing, cropping, RGB-to-grayscale conversion, Laplacian of Gaussian (LoG) filtering, Gabor filtering, global threshold segmentation, and image enhancement. A Convolutional Neural Network (CNN) is employed for classification purposes. Ninety percent of the images are allocated for training, while 10% are designated for testing, with critical parameters such as learning rate, batch size, and epochs being tuned throughout the training process. The CNN architecture was assessed based on recognition rate, error rate, epoch count, and training duration. The results provide a flawless validation accuracy of 100% over 32 trials. The findings demonstrate that the suggested method markedly enhances early breast cancer identification using microcalcification analysis in mammography images, assisting medical professionals in early diagnosis and potentially elevating patient recovery rates through prompt detection and treatment.

Keywords: breast cancer, Convolutional Neural Network, digital image processing, Gabor filter, mammography, microcalcification.

1. Introduction

Worldwide, cancer ranks high among the top killers. In 2018, there were 18.1 million new cases of cancer and 9.6 million deaths worldwide, according to figures from the World Health Organization (WHO) (World Health Organization, 2022). According to projections, the number of cancer-related deaths would surpass 13.1 million by 2030. Breast, lung, cervical, liver, lip, and oral cavity cancers were the leading causes of cancer-related fatalities among the 1.4 million cancer-related deaths and 2.2 million new cases recorded by the World Health Organization for the Southeast Asia region in 2015. Indonesia is facing a serious health crisis due to the alarmingly high incidence rates of breast cancer, the most common cancer in women. The most common cancer diagnosis in Indonesia in 2022 was breast cancer, with 408,661 new cases (International Agency for Research, 2022). Age, heredity, early menarche, reproductive history, obesity, alcohol use, and environmental variables are the main determinants of breast cancer risk. Breast cancer screenings, including self-examinations (SADARI, known as self-breast examinations by Indonesians), clinical breast exams (SADANIS, known as clinical breast examinations by Indonesians), and mammography, are an important part of primary and secondary preventive efforts. When it comes to finding breast cancer in its early stages, mammography is the imaging technique of choice. It involves both screening and diagnostic examinations aimed at identifying abnormalities in breast tissue and physical changes in the breast (Iranmakani, et al., 2020; Guzmán-Cabrera, et al., 2013; Sama & Baneamoon, 2017; Singh & Gupta, 2015; Basheer & Mohammed, 2013; Al-masni, et al., 2017). Mammography is highly sensitive in detecting lumps and microcalcifications, which can indicate the presence of abnormal cells or

© 2025 The Author(s). Published by Department of Information Systems and Technology, Universitas 17 Agustus 1945 Surabaya, Indonesia. This is an open access article under the CC BY-NC-ND license (https://creativecommons.org/licenses/by-nc-nd/4.0/), which permits use and distribution in any medium, provided the original work is properly cited, the use is non-commercial, and no modifications or adaptations are made.

malignant tumors (Logullo, Prigenzi, Nimir, Franco, & Campos, 2022).

Previous studies have shown that mammographic imaging techniques are highly effective in detecting breast cancer (Khoulqi & Idrissi, 2020). However, the visual limitations and subjectivity of human interpretation can lead to diagnostic inaccuracies. Therefore, the development of computer-based systems, particularly those employing artificial intelligence (AI), is essential to enhance diagnostic accuracy and efficiency. Machine learning and deep learning algorithms have been utilized in a number of studies to analyze mammographic images using artificial intelligence (Fadil, Jackson, Majd, Ghazi, & Kaabouch, 2019; Khoulqi & Idrissi, 2020). For example, Madhavi and Bobby's research showed that LS-SVM with Random Forest classification with Gabor filters produced very accurate and sensitive mammography results (Narasimhaiah & Nagaraju, 2023). Finding encouraging results, Khan and Arora investigated thermography utilizing Gabor filters and SVM classification as a non-invasive alternative to mammography (Salama & Aly, 2021). Combinations of machine learning algorithms based on Gabor filters have recently shown promising results in the identification of breast cancer (Podgornova & Sadykov, 2019; Wang, et al., 2024).

To advance these efforts, this study deliberately selects a combination of Gabor filters and a deep learning approach for specific, compelling reasons. The decision to employ Gabor filters is rooted in their exceptional ability to capture multi-scale and multi-orientation texture information. This characteristic is particularly advantageous for identifying microcalcifications, which often manifest as subtle, high-frequency textural patterns against a complex tissue background in mammograms. By simulating the response of the human visual cortex, Gabor filters excel at enhancing edges and local textural features, making them a powerful tool for preprocessing images to accentuate diagnostically relevant regions that might otherwise be missed (Kamil, 2020).

Furthermore, this study adopts a Convolutional Neural Network (CNN), a state-of-the-art deep learning architecture, to address the limitations of traditional machine learning approaches. Unlike conventional methods that rely on manually engineered features, CNNs offer the distinct advantage of automatically learning hierarchical feature representations directly from the image data. Through this end-to-end learning process, the model is able to capture intricate and abstract patterns indicative of malignancy, ranging from simple edges in the early layers to more complex shapes in the deeper layers. This capability renders CNNs particularly robust and effective for complex medical image classification tasks.

This research, therefore, proposes a synergistic methodology that combines the targeted feature enhancement of Gabor filters with the powerful automated classification of CNN (Annisa, Lubis, & Najmita, 2020; Fuadi, 2023). The goal is to develop a highly accurate system for early breast cancer detection by analyzing microcalcifications in the Mini-DDSM dataset. By integrating these advanced techniques, this study aims to improve the manual interpretation of mammographic pictures, provide a reliable decision support tool for medical practitioners, and ultimately contribute to increasing patient recovery rates through more timely and precise diagnosis (Alfayat & Whardana, 2024; Whardana, Mufti, Hermawan, & Aziz, 2024; Whardana & Putri, 2025).

2. Theoretical Background

Subsection 2.1 will offer a comprehensive overview of the definition, progression, and essential characteristics of breast cancer to elucidate the principles and mechanisms of breast cancer detection methods.

2.1. Breast Cancer

Cancer develops when normal cells sustain DNA damage, leading to alterations in their DNA. These cells alter and start to proliferate and expand faster than usual. After a certain age, cancer cells stop replicating and become invasive, suppressing or even killing off healthy cells in the body. According to American Cancer Society, breast cancer is a specific kind of cancer that develops in the breast's supporting tissues, glandular cells, and glandular ducts; nevertheless, it does not affect the breast skin (American Cancer Society, 2014).

2.2. Mammography

Breast cancer is a malignancy that affects the mammary glands and adjacent tissues within the breast. To mitigate the risk of breast cancer, early screening, including medical evaluations as outlined by Dyanti & Suariyani (2016), is essential. In this context, a prevalent diagnostic technique employed by physicians is mammography, which utilizes X-rays as a light source to generate images. The output produced from this mammography assessment is designated as a mammographic image, as seen in Fig. 1 (Brahimetaj, et al., 2022; Cardona, Orozco, & Álvarez, 2014; Zamir, et al., 2021; Leong, Hasikin, Lai, Zain,

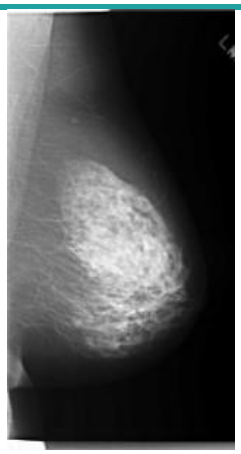

Fig. 1. Breast mammography image.

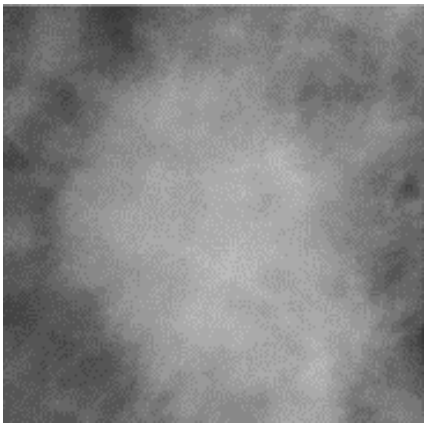

Fig. 2. Mass mammography image.

& Azizan, 2022).

Mammography is a medical imaging procedure that utilizes low-dose X-rays to visualize the internal structure of breast tissue, producing what is known as a mammographic image. The image highlights different densities, with glandular tissue appearing as bright white areas due to higher density, while fatty tissue appears darker. This type of imaging is essential for early detection and diagnosis of breast cancer, as it allows for the identification of abnormalities such as irregular masses, blurred boundaries, or grouped microcalcifications. Early detection through mammography significantly improves the chances of successful treatment by identifying cancer before clinical symptoms emerge. Additionally, digital mammography has enhanced image resolution and introduced tools like Computer-Aided Detection (CAD) systems, which help radiologists identify suspicious areas with greater accuracy. As a non-invasive diagnostic method, mammography is a cornerstone in breast cancer screening programs, particularly for women over 40 or those with genetic predispositions, offering a critical advantage in reducing breast cancer mortality rates (Guo, et al., 2022; Liew, Hameed, & Clos, 2021; Zhao, Chen, & Cai, 2022).

2.3. Types of Breast Cancer

Mammographic images are crucial for detecting breast cancer, especially through the identification of mass lesions, known as masses, and the detection of microcalcifications. On mammography, breast cancers, whether benign or malignant, typically manifest as lumps. A mass denotes a region containing a lesion observable from two distinct projections in mammographic imaging, as illustrated in Fig. 2.

The presence of microcalcifications is an additional characteristic of breast cancer. The deposition of calcium minerals in breast tissue, known as lobular or ductal tissue, results in microcalcifications that appear as minute stains or patches. Fig. 3 illustrates that microcalcifications serve as a significant signal of potential breast cancer in mammographic images.

Using mammography technology, doctors can more thoroughly and precisely identify the type of breast cancer, providing a solid basis for further diagnosis and appropriate treatment planning. Awareness of the importance of understanding the type of breast cancer through mammography images is the first step in early detection and effective treatment of this disease.

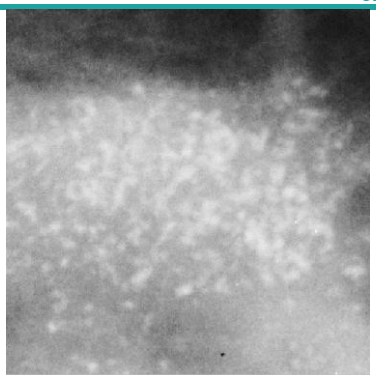

Fig. 3. Microcalcification mammography image.

2.4. Digital Image Processing

Digital image processing involves analyzing images using computer algorithms to enhance image quality, extract embedded data, and transform images for easier human interpretation or analysis. It begins with two core implementations: improving visual data for accurate interpretation and organizing visual information for autonomous device recognition. The primary focus of the latter is to extract visual data in a computer-processable format. An image can be viewed as a 2D function of light intensity, $f(x, y)$, with spatial coordinates (x, y) representing positions in the image plane. The brightness or gray level at each point (x, y) corresponds to the value of f. Image processing is generally categorized into three types: low-level, mid-level, and high-level processing. Low-level processing includes basic operations like image rotation, reading, resizing, histogram normalization, and color conversion, which modify the original image. Mid-level processing involves extracting information from low-level processes, such as edge detection. High-level processing enhances mid-level processing with artificial intelligence integration (Singh & Goel, 2020).

3. Methods

The research methodology employed in this study is meticulously designed to ensure a comprehensive analysis and accurate results. This section provides an in-depth explanation of the processes and techniques applied throughout the research. The methodical approach encompasses various stages, from data collection and preprocessing to the implementation and evaluation of advanced machine learning models. Each step is carefully orchestrated to ensure precision and reliability, thereby enhancing the overall validity of the study's findings. The following subsections detail these processes, beginning with the system flowchart that provides a visual representation of the workflow.

3.1. System Flowchart

We design the system flowchart whose main function is to provide a better understanding of the processes that occur within the system. Fig. 4 is the system flowchart design used in breast cancer early detection research through microcalcification analysis with Gabor filters and deep learning Convolutional Neural Network (CNN) (Mohimont, Alin, Rondeau, Gaveau, & Steffenel, 2022; Zhang & Lu, 2021; Sarker, 2021; Fuadi, 2023).

3.2. Dataset Collection and Selection

The secondary dataset used in this research was obtained from Kaggle, an open-source platform that provides publicly available medical imaging resources. Specifically, the dataset is the Mini Digital Database for Screening Mammography (Mini-DDSM), a compressed version of the original DDSM curated by the University of South Florida (USF). This collection contains 9,684 PNG-formatted mammography images sourced from patients aged 25 to 90 years (median age of 50), categorized into three classes: 2,728 Normal, 3,360 Benign, and 3,596 Cancer cases. During the dataset selection stage, images with edge noise that could affect preprocessing were removed. After the refinement process, a total of 8,914 images were retained, consisting of 2,544 Normal, 3,006 Benign, and 3,364 Cancer samples, which were subsequently used for preprocessing and model training. Examples of the dataset categories are presented in Fig. 5.

3.3. Preprocessing

The preprocessing of mammography images consists of several essential steps aimed at improving image quality before classification using Convolutional Neural Networks (CNN). These steps are designed to minimize noise or artifacts that may interfere with diagnostic accuracy. The process begins with resizing all images to a standardized resolution of 512 × 512 px using MATLAB's imresize function, ensuring uniform

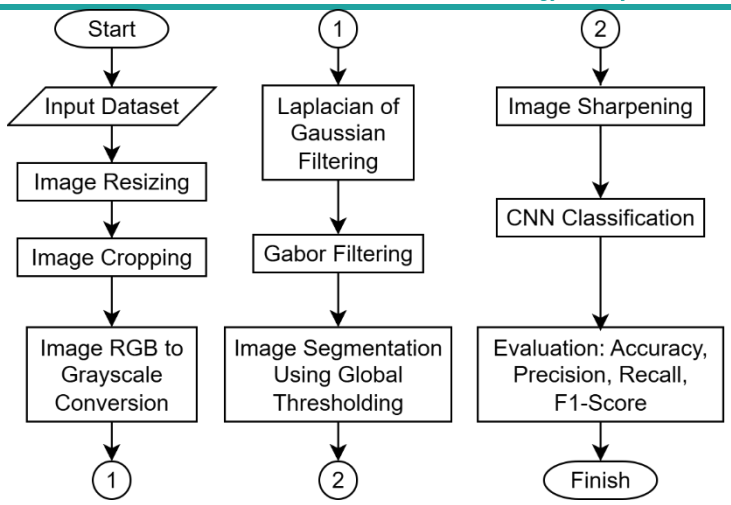

Fig. 4. Flowchart of the proposed classification method.

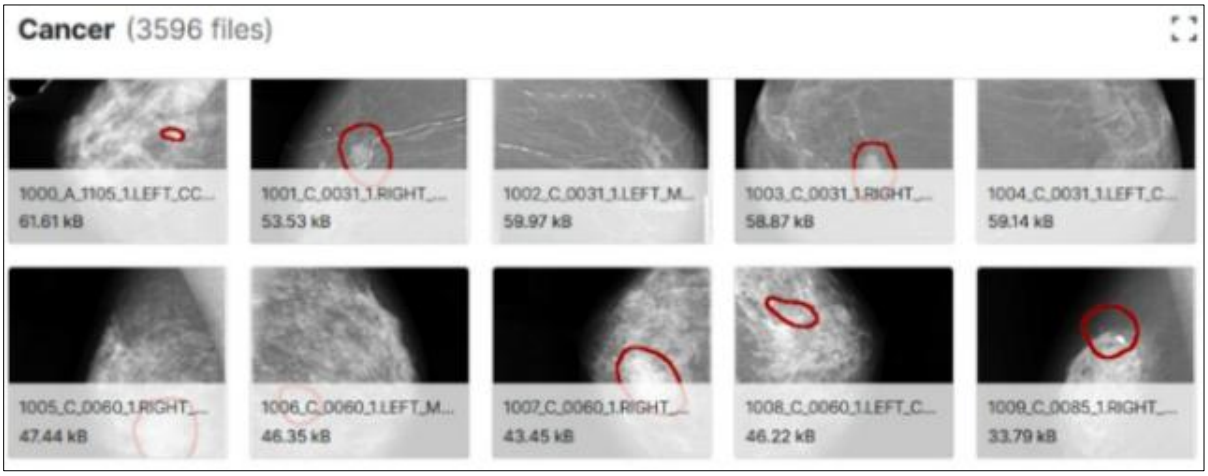

Fig. 5. Example of Kaggle Mini-DDSM dataset.

dimensions and eliminating unnecessary variations across the dataset. The overall workflow of this preprocessing stage is illustrated in Fig. 4, where each step is systematically arranged to prepare the images for further enhancement and feature extraction. Following the resizing step, the next stage involves image cropping, which focuses on removing irrelevant regions and retaining diagnostically significant breast tissue areas for subsequent analysis.

As illustrated in Fig. 4, the preprocessing pipeline systematically organizes the key steps required before classification. Starting from the dataset input, the images undergo resizing, cropping, and grayscale conversion to standardize their format. Subsequent filtering techniques, such as Laplacian of Gaussian and Gabor filters, are applied to enhance edge details and capture texture-based features. Additional processes, including threshold segmentation and image sharpening, further refine the data by reducing noise and emphasizing diagnostically relevant structures. This sequential workflow ensures that the input images are optimized for CNN classification, ultimately supporting more accurate and reliable detection of breast abnormalities.

Fig. 6 presents the flowchart of the CNN model used for training in this study. The diagram outlines the sequential process beginning with the input of preprocessed mammography images, followed by splitting the dataset into training and testing sets, initializing learning parameters, and proceeding with CNN training (Nagane & Mulani, 2021). The final stage produces classification outputs into three categories: Benign, Cancer, and Normal. This flow complements the architectural details summarized in Table 3, where each convolutional, pooling, and fully connected layer contributes to feature extraction and decision-making. Together, the flowchart and the architectural table provide a comprehensive view of how the CNN model is structured and executed to achieve reliable breast cancer image classification (Jothiaruna, Sundar, & Ahmed, 2021; Kadir, Nugroho, Susanto, & Santosa, 2011; Saifullah, Sunardi, & Yudhana, 2016; Iriyanto & Zaini, 2014; Annisa, Lubis, & Najmita, 2020).

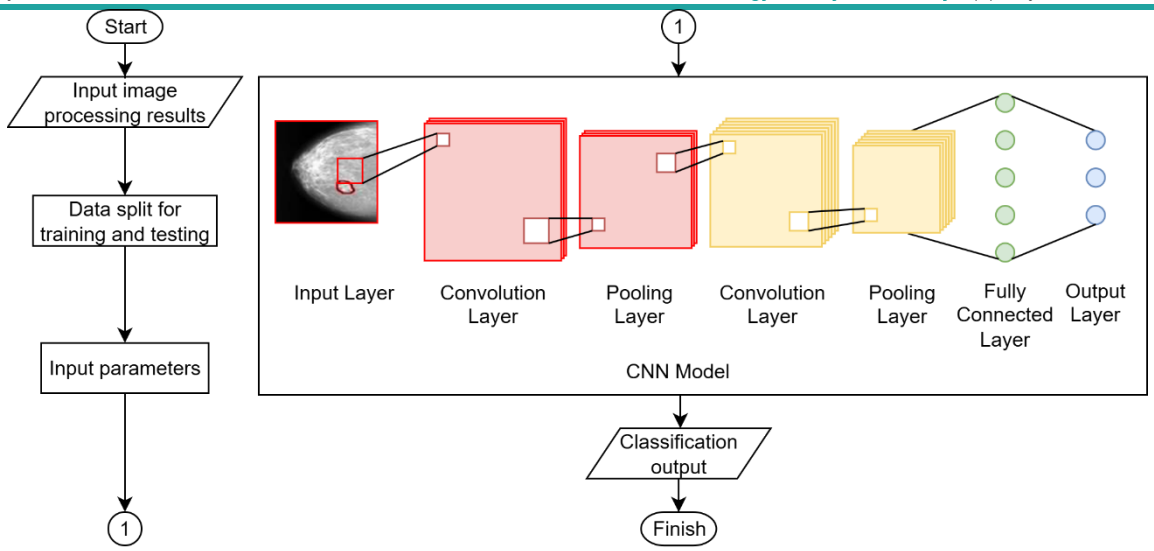

Fig. 6. Flowchart of the training process for the Convolutional Neural Network (CNN) model. The illustration of the CNN model is inspired by Gu, Wang, Hong, & Gui (2019).

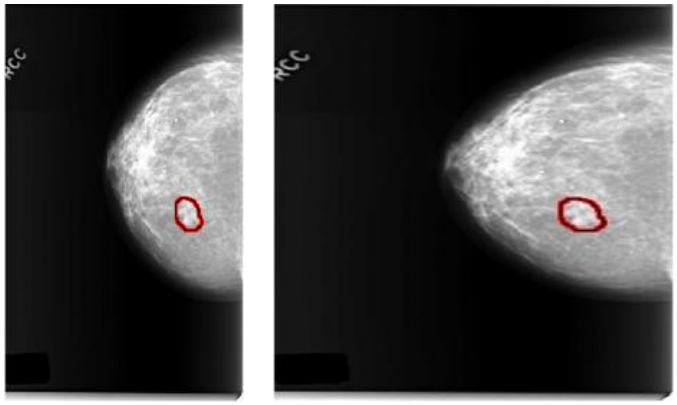

(a) (b)

Fig. 7. Image preprocessing steps: (a) Original image, and (b) Resized image.

3.3.1. Image resizing

Image preprocessing is a fundamental step in the development of image-based machine learning models, particularly in medical imaging. This step ensures the consistency, quality, and usability of the input data for subsequent processing and analysis. By standardizing various image attributes such as size, resolution, and intensity, preprocessing facilitates accurate feature extraction and model training. This process is essential for eliminating variability in raw data and improving the robustness and generalizability of the model. One of the critical preprocessing operations applied in this study is image resizing, which is discussed in the following subsection.

Image resizing changes the mammography image to a size of 512 x 512, which aims to equalize the size of the obtained image and prepare it for input to training using a Convolutional Neural Network (CNN). The example result of the image that has been resized is shown in Fig. 7.

Fig. 7 illustrates the outcome of the image resizing process as part of the image preprocessing stage. Fig. 7(a) shows the original mammography image, while Fig. 7(b) depicts the resized image with dimensions standardized to 512 × 512 px. This resizing step is essential for ensuring uniformity across all input images, thereby facilitating efficient and consistent training using CNNs. The comparison between the original and resized images highlights the importance of this preprocessing step as it enhances the performance of subsequent image analysis and model training phases.

3.3.2. Image cropping

The next preprocessing step in this study is image cropping. After resizing each mammography image to 512 × 512 px, cropping is applied to remove extraneous artifacts such as watermarks and to retain only the relevant breast tissue region. This operation produces an image of 512 × 450 px, as illustrated in Fig. 8, thereby improving focus and reducing noise for subsequent feature extraction and classification.

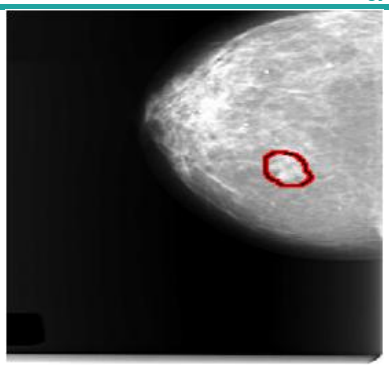

Fig. 8. Image preprocessing: Example of a cropped image.

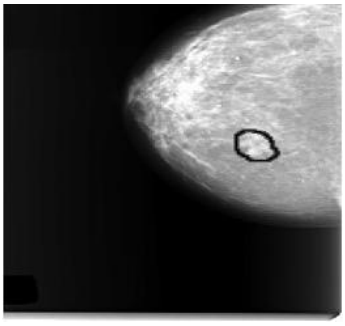

Fig. 9. Image Preprocessing: Example of image grayscale result.

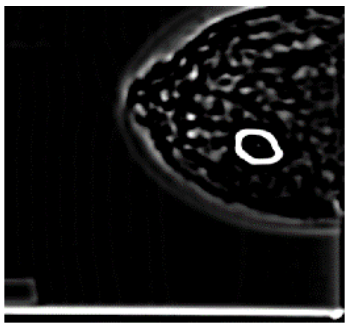

Fig. 10. Image preprocessing: Example of a grayscale-converted image.

Fig. 8 presents the cropping result of mammography images, focusing on the region of interest (ROI). This step isolates the relevant breast tissue area while eliminating background information that may introduce noise. Highlighting the ROI supports more accurate feature extraction, thereby improving the performance of subsequent classification tasks.

3.3.3. Red, Green, Blue (RGB) to Grayscale Conversion

The next preprocessing step in this study is the conversion of mammography images from Red, Green, and Blue (RGB) format to grayscale. Fig. 9 shows a grayscale image. This transformation is necessary because mammography images are inherently grayscale, and the presence of RGB pixels can cause unnecessary variation. Converting the image to grayscale eliminates this inconsistency, resulting in a uniform black-and-white representation.

Fig. 9 presents the result of converting the mammography image from RGB to grayscale. This preprocessing is necessary because mammographic images are inherently grayscale; residual RGB pixels may introduce unwanted variation. The conversion removes these discrepancies and produces a uniform black-and-white representation that improves contrast and highlights diagnostically relevant structures for later analysis.

3.3.4. Laplacian of Gaussian (LoG) filtering

The Laplacian of Gaussian (LoG) filter was applied in this study to sharpen the edges of mammography images and highlight the Region of Interest (ROI). This method was designed to improve the visibility of disturbances or abnormalities in breast tissue, thereby supporting the identification of potential abnormalities. The ROI references were obtained from the Mini-DDSM dataset available on Kaggle, which

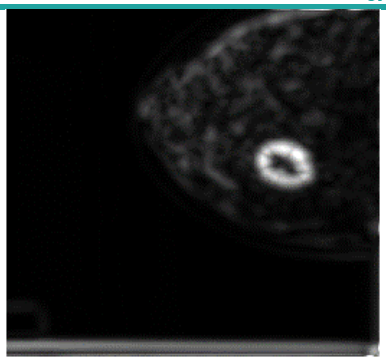

Fig. 11. Gabor filter process.

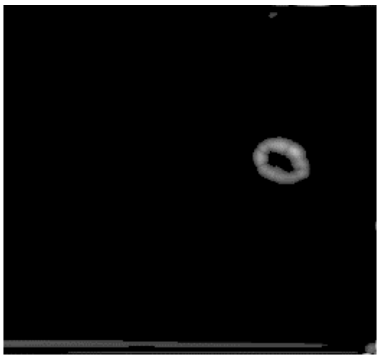

Fig. 12. Global threshold segmentation.

was curated by radiographers. In this study, the LoG parameters were set with a filter size of 50 and a Gaussian scale (σ) of 5, which controls the spread of light values on pixels. Fig. 10 shows the results of applying the LoG filter (Ghosal, Mandal, & Sarkar, 2018).

Fig. 10 presents the result of applying the LoG filter to a mammography image. The filter successfully enhances the edges of breast tissue structures and clearly delineates the ROI. This enhancement facilitates the identification of potential abnormalities by improving contrast and highlighting diagnostically significant features, thereby supporting subsequent stages of image analysis and classification.

3.3.5. Gabor filtering

The Gabor filter is one of the most important preprocessing steps in this study, as it extracts texture-based features that capture the orientation of pixel intensity variations in the image. Fig. 10 shows the Gabor filter process. This process improves the visibility of microcalcifications in mammography images by highlighting directional patterns. This filter operates using two main parameters: wavelength (λ), which determines the spatial frequency of light that can be detected, and orientation (θ), which determines the direction of the wave (Kamil, 2020). In this study, the wavelength was set to 3.5, while four orientations were applied at 0°, 45°, 90°, and 135°, enabling the detection of microcalcifications in various directional fields.

Fig. 11 illustrates the outcome of applying the Gabor filter to a mammography image during the preprocessing stage. The filter enhances the detection of microcalcifications by emphasizing texture and edge details in multiple orientations. The directional patterns generated through the Gabor filter highlight diagnostically significant structures, thereby facilitating more accurate feature extraction and supporting subsequent classification and analysis.

3.3.6. Global threshold segmentation

After the application of the Gabor filter, this study employed global threshold segmentation to further refine the image quality. This technique reduces noise by distinguishing between foreground and background pixels based on a fixed threshold value (Houssein, Helmy, Oliva, Elngar, & Shaban, 2021). In this study, a threshold value of 0.4 was selected to suppress irrelevant artifacts, such as dust particles, that could obscure diagnostically significant features. This step ensures greater focus on microcalcification regions, thereby enhancing their structural visibility for subsequent classification tasks. The result of this process is presented in Fig. 12.

The outcome of the global threshold segmentation is presented in Fig. 12, which demonstrates the effective separation of foreground and background pixels in the mammography image. The application of a threshold value of 0.4 successfully suppresses irrelevant noise, such as dust artifacts, and highlights diag-

Fig. 13. Image sharpen result.

Table 1
Dataset distribution for preprocessing, labeling, and data splitting.

Label	Total Samples	Training Data (90%)	Testing Data (10%)
Benign	3,006	2,290	254
Cancer	3,364	2,705	301
Normal	2,544	3,028	336

Table 2
Training results at varying learning rates, epochs, mini-batch sizes, and validation frequencies.

Learning Rate	Epochs	Mini-Batch Size	Validation Frequency	Training Time (min:s)	Validation Accuracy (%)
0.05	10	10	10	36:24	37.71
0.05	10	10	50	12:33	33.78
0.05	10	50	10	12:34	37.71
0.05	10	50	50	09:05	37.71
0.05	20	10	10	84:17	33.78
0.05	20	10	50	25:30	33.78
0.05	20	50	10	24:26	37.71
0.05	20	50	50	54:59	37.71
0.01	10	10	10	30:09	37.71
0.01	10	10	50	12:35	33.78
0.01	10	50	10	12:41	100.00
0.01	10	50	50	08:48	37.71
0.01	20	10	10	60:30	37.71
0.01	20	10	50	25:04	37.71
0.01	20	50	10	25:06	100.00
0.01	20	50	50	17:25	100.00
0.005	10	10	10	32:06	37.71
0.005	10	10	50	12:36	37.71
0.005	10	50	10	12:48	99.66
0.005	10	50	50	09:28	99.66
0.005	20	10	10	62:05	99.33
0.005	20	10	50	24:45	100.00
0.005	20	50	10	25:04	100.00
0.005	20	50	50	17:27	100.00
0.001	10	10	10	34:41	100.00
0.001	10	10	50	13:31	100.00
0.001	10	50	10	13:19	100.00
0.001	10	50	50	09:10	100.00
0.001	20	10	10	60:21	100.00
0.001	20	10	50	24:38	99.66
0.001	20	50	10	26:45	99.66
0.001	20	50	50	18:28	99.55

nostically significant regions. As shown in the figure, this method isolates the microcalcification area with greater clarity, thereby enhancing structural visibility and improving the reliability of subsequent image classification tasks.

Table 3
Layers' description for the proposed CNN architecture.

Layer	Kernel/Units	Stride	Output Shape
0 Input	-	-	512 × 450 × 1
1 Conv2D	3 × 3, 8 filters	1	512 × 450 × 8
2 BatchNorm + ReLU	-	-	512 × 450 × 8
3 MaxPool2D	2 × 2	2	256 × 225 × 8
4 Conv2D	3 × 3, 16 filters	1	256 × 225 × 16
5 BatchNorm + ReLU	-	-	256 × 225 × 16
6 MaxPool2D	2 × 2	2	128 × 112 × 16
7 Conv2D	3 × 3, 32 filters	1	128 × 112 × 32
8 BatchNorm + ReLU	-	-	128 × 112 × 32
9 Flatten/ GlobalAvgPooling2D	-	-	Vector (128 × 112 × 32)
10 Dense (Classifier)	3 units	-	3
11 Softmax	-	-	3 (class probabilities)

3.3.7. Image sharpening

The image sharpening process is applied to enhance the quality of mammography images by increasing edge definition and improving the clarity of diagnostically relevant structures. This method utilizes the Image Sharpen function in MATLAB to emphasize fine details and highlight the boundaries of microcalcifications, thereby supporting more accurate analysis in subsequent stages. As shown in Fig. 13, the sharpening process produces a clearer and more focused representation of the breast tissue, enabling better identification of critical features while reducing ambiguity in the image interpretation.

Fig. 13 shows the result of applying the Image Sharpen method to mammography images. This process enhances fine details and clarifies the boundaries of microcalcifications, making the structures more distinct and easier to interpret. By improving visual sharpness, this step strengthens the accuracy of subsequent analysis, particularly in identifying critical features within breast tissue.

After the preprocessing stage, all images produced through the Image Sharpen process are categorized into three classes: Benign, Cancer, and Normal, as presented in Table 1. From a total of 8,914 available images, the dataset is split into 90% for training and 10% for testing. This splitting provides a balanced representation of each class, ensuring that the Convolutional Neural Network (CNN) model can be trained with an appropriate data distribution.

Furthermore, the results of CNN training using the dataset were evaluated under various combinations of learning rate parameters, number of epochs, mini-batch size, and validation frequency (VF). Table 2 summarizes the model performance for each configuration. The results indicate that models trained with a relatively large learning rate of 0.05 yielded low and unstable validation accuracy. In contrast, smaller learning rates of 0.01, 0.005, and 0.001 achieved significantly higher accuracy, with some configurations reaching 99–100%. These findings highlight the critical role of selecting appropriate training parameters to optimize CNN performance in mammography image classification.

These experimental outcomes confirm that the adjustment of learning rate parameters has a substantial impact on model performance. By identifying optimal configurations that achieve stable and high validation accuracy, the study establishes a strong foundation for the subsequent CNN training and evaluation stages.

3.4. Convolutional Neural Network (CNN)

The deep learning process using Convolutional Neural Network (CNN) for mammography image analysis in this study was carried out through a structured sequence, beginning with data preprocessing and continuing to performance evaluation. To support this process, a lightweight CNN architecture was developed, consisting of three convolutional blocks followed by a classifier head (Brian, 2016; Basheer & Mohammed, 2013). The input to the model is a grayscale mammography image resized to 512 × 450 × 1. Each convolutional block employs a 3×3 convolutional kernel with "same" padding, followed by Batch Normalization and ReLU activation to stabilize training and introduce non-linearity. In the first two blocks, 2×2 max-pooling is applied to progressively reduce spatial dimensions while preserving essential features. The final stage of the network consists of a fully connected, dense layer with a softmax activation function, which produces probability outputs for the three target classes: Benign, Cancer, and Normal. The detailed specification of this CNN architecture, including filter sizes, strides, and output dimensions for each layer, is presented in Table 3.

After splitting the dataset into training and testing sets, the initialized parameters (learning rate (LR), batch size (BS), and epochs) were applied to guide the training process. The CNN model was then trained using the proposed architecture summarized in Table 1, enabling the network to learn discriminative features and generate classification outputs for mammography images (Madhavi & Bobby, 2019; Khan & Arora, 2019; Moyya & Asaithambi, 2022).

3.5. Performance Measures

The performance of the CNN classification was evaluated using a confusion matrix, which categorizes predictions into four distinct outcomes: True Positives (TP), True Negatives (TN), False Positives (FP), and False Negatives (FN). By analyzing these outcomes, we can derive critical metrics such as accuracy, precision, recall, and F1-score, which provide a comprehensive understanding of the model's efficacy in distinguishing between different classes. This evaluation is instrumental in refining the model and enhancing its predictive capabilities. The evaluation metrics are defined by the following equations:

- Accuracy: Indicates overall correctness.
  As shown in Eq. (1) (Gupta, Anjum, Gupta, & Katarya, 2021), accuracy quantifies the overall correctness of the model's predictions. The accuracy is computed by dividing the sum of true positives (TP) and true negatives (TN) by the total number of predictions, including true positives, true negatives, false positives (FP), and false negatives (FN). This metric provides a broad assessment of the model's performance and serves as a foundational measure for evaluating classification systems.

$$Accuracy = \frac{TP + TN}{TP + TN + FP + FN} \quad (1)$$

- Precision: Reflects the reliability of positive predictions.

$$Precision = \frac{TP}{TP+FP} \quad (2)$$

  Eq. (2) defines precision (Gupta, Anjum, Gupta, & Katarya, 2021), which assesses the reliability of the model's positive predictions. Precision is calculated as the ratio of true positives (TP) to the total number of predicted positive cases, including true positives and false positives (FP). A higher precision, as indicated by this equation, reflects a low false positive rate, signifying that the model consistently identifies true positives with minimal errors. This metric is especially critical in scenarios where false positives carry significant consequences.
- Recall: Measures the correct identification of positive cases.

$$Recall = \frac{TP}{TP + FN} \quad (3)$$

  As outlined in Eq. (3) (Gupta, Anjum, Gupta, & Katarya, 2021), recall (or sensitivity) measures the model's ability to correctly identify positive cases. It is derived by dividing the number of true positives (TP) by the sum of true positives and false negatives (FN). A high recall value, as expressed by the formula, indicates that the model successfully detects a large proportion of actual positive cases, minimizing false negatives. This metric is particularly important in applications where failing to identify positive instances has serious implications, such as medical diagnostics.
- F1-score: Provides a harmonic mean of precision and recall.
  The F1-score (Gupta, Anjum, Gupta, & Katarya, 2021), calculated as shown in Eq. (4), represents the harmonic mean of precision and recall, offering a balanced evaluation of the model's performance. This metric is especially valuable when dealing with imbalanced datasets, as it combines both precision and recall into a single value that accounts for the trade-off between these two metrics. A high F1-score, derived from this formula, indicates that the model performs well in identifying positive cases without compromising reliability or sensitivity.

$$F1 - Score = 2 \times \frac{Precision \times Recall}{Precision + Recall} \quad (4)$$

4. Results and Discussion

This section delves into the findings derived from the research and their comprehensive evaluation. The analysis and interpretation of these results are crucial for understanding the effectiveness and robustness of the methodologies employed. By examining the outcomes in detail, we can assess the performance of the proposed approaches, identify potential areas for improvement, and draw meaningful conclusions about the practical implications of the study. The results are presented in a structured manner,

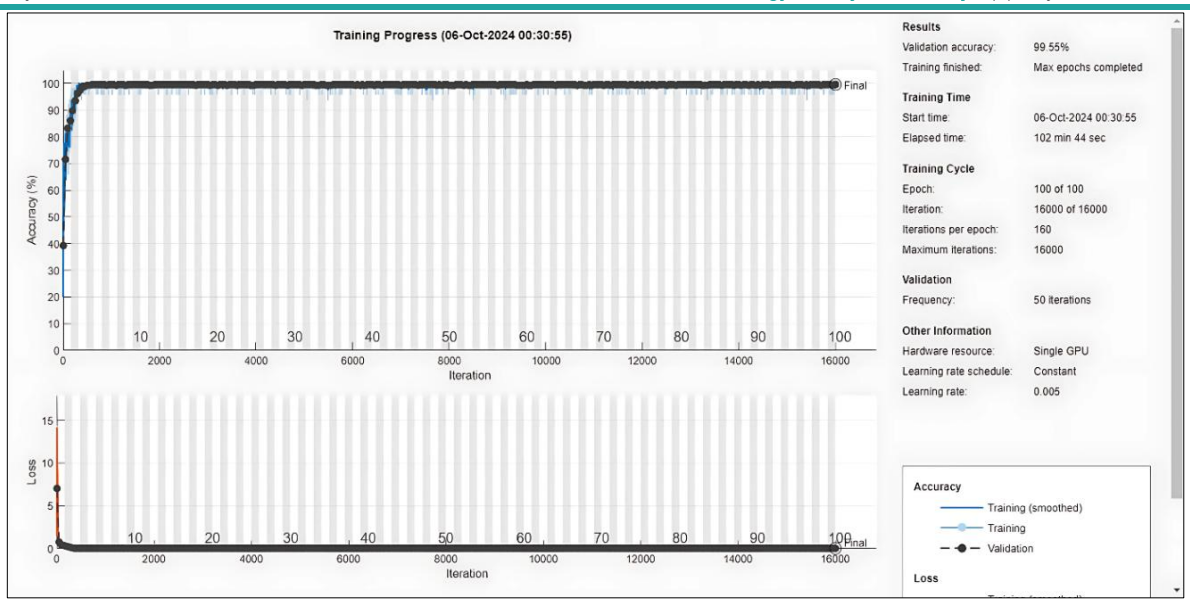

Fig. 14. With a learning rate of 0.005, the Convolutional Neural Network achieved an accuracy of 99.55%.

beginning with the dataset collection and followed by image preprocessing, model training, and performance evaluation. Each subsection provides a thorough examination of the respective steps, supported by relevant figures and tables, and quantitative metrics, to offer a clear and coherent narrative of the research findings.

4.1. Preprocessing Results

The preprocessing phase is essential for preparing mammography images for subsequent feature extraction and classification. Each step is designed to enhance the diagnostic quality of the images by removing extraneous artifacts, improving contrast, and highlighting diagnostically relevant structures. The results of these procedures are sequentially presented in Figs. 7–13, with each figure illustrating the transformation applied at a specific stage of the preprocessing pipeline.

The procedure begins with image resizing (Fig. 7) to standardize all images to a uniform resolution of 512 × 512 pixels. This is followed by image cropping (Fig. 8) to remove extraneous artifacts such as watermarks and retain only the breast tissue region. Next, the images are converted from RGB to grayscale (Fig. 9), ensuring consistency by eliminating unnecessary color variations. The Laplacian of Gaussian (LoG) filter (Fig. 10) is then applied to enhance important edges and highlight microcalcifications. This is followed by the Gabor filter (Fig. 11), which extracts orientation-based texture features relevant to detecting abnormalities. Global threshold segmentation (Fig. 12) is subsequently used to reduce noise further and delineate regions of interest, while the image sharpening step (Fig. 13) enhances the clarity of fine structural details. This comprehensive preprocessing pipeline demonstrates how each step progressively improves image quality, ensuring that the final dataset input into the CNN is standardized, reliable, and diagnostically meaningful.

4.2. Training and Validation Results

This study utilized a dataset comprising 8,914 mammography images, which were preprocessed and classified into three diagnostic categories: Benign, Cancer, and Normal. The dataset was split into two subsets to facilitate effective and representative model training, with 90% (8,027 images) allocated for training and 10% (887 images) reserved for testing. This partitioning ensures sufficient data for training while maintaining an independent set for unbiased performance evaluation. Detailed distribution of images per category is presented in Table 1.

The Convolutional Neural Network (CNN) was trained using diverse parameter configurations, with a primary emphasis on the learning rate, batch size, and number of epochs. Table 2 delineates the validation accuracy and training duration attained under these conditions. The findings suggest that models trained with a comparatively elevated learning rate (0.05) exhibited inconsistent performance, yielding validation accuracies between 33% and 37%. In contrast, reduced learning rates (0.01, 0.005, and 0.001) consistently produced markedly higher validation accuracy, achieving up to 99–100% in specific configurations. This discovery underscores the significance of selecting a reduced learning rate to facilitate more successful convergence of the network.

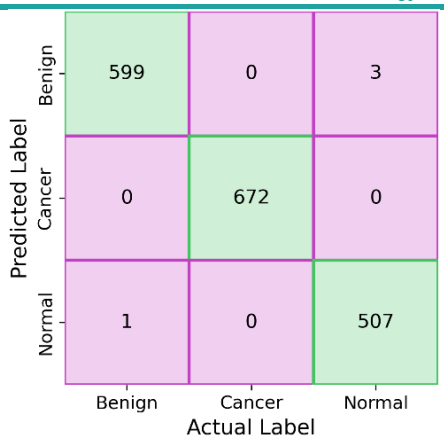

Fig. 15. Confusion matrix for CNN classification on the test dataset (Learning Rate = 0.005).

Table 4
Convolutional Neural Network (CNN) classification results and evaluation.

LR	Epoch	BS	VF	Time (min:s)	Acc. Val. (%)	Prec. Benign (%)	Prec. Cancer (%)	Prec. Normal (%)	Rec. Benign (%)	Rec. Cancer (%)	Rec. Normal (%)	Mic. Prec. (%)	Mic. Rec. (%)	Mic. F1 (%)
0.005	100	50	50	102:44	99.55	99,50	100	99.80	99.83	100	99.41	99.78	99.78	99.78

Notes: Accuracy (Acc.), Precision (Prec.), Recall (Rec.), Micro-Averaged Precision (Mic. Prec.), Micro-Averaged Recall (Mic. Rec.), and Micro-Averaged F1-score (Mic. F1).

The number of epochs was evaluated at both 10 and 20. The findings indicate that prolonging training to 20 epochs did not uniformly enhance accuracy, implying that the model had already attained convergence prior to the maximum iteration count. This suggests that extending epochs beyond a specific limit may not enhance performance, but instead prolongs processing time.

The batch size significantly influenced efficiency and performance. Larger batch sizes, such as 50, generally decreased training time per epoch, but did not consistently produce higher accuracy compared to smaller batch sizes, such as 10. This finding suggests that smaller batch sizes may facilitate more precise parameter updates during training, although this comes with increased computational costs.

Fig. 14 depicts the training process and validation curves, demonstrating a swift improvement in accuracy during the initial iterations, which subsequently stabilized near 100% after roughly 2,000 iterations. Simultaneously, the loss value diminished and settled around zero, further validating the efficacy of the selected hyperparameters.

The findings collectively demonstrate that the optimal configuration for this model was achieved with a learning rate of 0.005, a batch size of 50, and 10–20 epochs, resulting in the most advantageous equilibrium between accuracy (99.55%) and computational efficiency. These findings underscore the critical significance of hyperparameter optimization in improving CNN efficacy for mammography image classification. The adjusted hyperparameters were later utilized in the final evaluation with the independent testing set, and the results are displayed in Fig. 15 and Table 4.

4.3. CNN Architecture and Performance Evaluation

The Convolutional Neural Network (CNN) used in this study was designed as a lightweight architecture consisting of three convolutional blocks followed by a classifier head. The input to the model is a grayscale mammography image resized to 512 × 450 × 1, ensuring uniformity across the dataset. Each convolutional block applies a 3 × 3 kernel with same padding, followed by Batch Normalization and ReLU activation to stabilize training and introduce non-linearity. In the first two blocks, 2 × 2 max-pooling is applied to reduce the spatial dimensions while preserving essential features progressively.

The final stage of the network consists of a fully connected dense layer with a softmax activation function, producing three probability outputs corresponding to the target classes: Normal, Benign, and Cancer. The overall workflow of the CNN training process is summarized in Fig. 14, which illustrates the sequence from data input and preprocessing to training and classification. The detailed layer-by-layer configuration of the proposed CNN model is presented in Table 2, including kernel sizes, strides, and output dimensions.

Moreover, the architecture was deliberately crafted to attain an equilibrium between computing efficiency and diagnostic precision. The model has a shallow architecture of three convolutional blocks, hence reducing the likelihood of overfitting while ensuring computational efficiency for extensive

mammography datasets. The incorporation of Batch Normalization and ReLU activation within each block improves stability and expedites convergence, while the softmax output layer offers interpretable probability distributions for clinical decision assistance. This approach guarantees that the CNN effectively captures essential texture and edge-related data while providing robust and dependable classification across the three diagnostic categories.

Fig. 14 illustrates that the training process of the CNN model exhibits a rapid increase in accuracy during the initial iterations, reaching stable convergence after approximately 2,000 iterations. The validation accuracy achieved 99.55%, while the loss value steadily decreased and stabilized near zero, indicating that the model successfully minimized classification errors without signs of overfitting. The close alignment between training and validation curves further confirms the robustness of the selected parameters, particularly the learning rate (LR) of 0.005, which facilitated both high accuracy and effective convergence. These findings affirm that the proposed CNN architecture is capable of distinguishing between normal, benign, and malignant mammography images with high reliability, thereby validating the preprocessing pipeline and model configuration.

Following the strong training performance shown in Fig. 14, the model was then evaluated on the unseen testing dataset to assess its generalization ability. The evaluation results, summarized in the confusion matrix presented in Fig. 15, demonstrate that the CNN achieved highly accurate classification across all three categories. Specifically, the model correctly identified 599 Benign, 672 Cancer, and 507 Normal instances, with only four misclassifications in total (three benign images predicted as normal and one normal image predicted as benign). This corresponds to a test micro-accuracy of 99.78%, with per-class F1-scores of 99.67% (Benign), 100.00% (Cancer), and 99.61% (Normal). The overall macro-F1 score reached 99.76%, while the weighted-F1 score was 99.78%. These results underscore the effectiveness of the proposed CNN model in accurately classifying mammography images and highlight its robustness for practical application in early breast cancer detection.

Fig. 15 displays the confusion matrix for the CNN classification applied to the testing dataset, utilizing a learning rate of 0.005. The algorithm attained exceptional predictive accuracy, properly classifying 599 Benign, 672 Cancer, and 507 Normal pictures, with merely four occurrences misclassified (three benign cases identified as normal and one normal case identified as benign). The results demonstrate the model's robust ability to differentiate among the three diagnostic categories with negligible error. Table 4 presents a comprehensive assessment of performance indicators, encompassing accuracy, precision, recall, and F1-score for each category, based on these results. The model achieved a validation accuracy of 99.55%, with per-class precision and recall metrics regularly exceeding 99%, and an overall F1-score of 0.9975. The uniformity across several evaluation parameters validates both the resilience of the proposed CNN architecture and the efficacy of the preprocessing pipeline in generating dependable and diagnostically significant classifications.

Table 4 illustrates the exceptional reliability and robustness of the proposed CNN model in the classification of mammography pictures. The model exhibits exceptional generalization to unknown data, evidenced by a validation accuracy surpassing 99% and consistently high precision, recall, and F1-scores across all classes. The results validate that the preprocessing pipeline, in conjunction with the lightweight CNN architecture, establishes a very efficient framework for the early identification of breast cancer. This evaluation is followed by an explanation that elaborates on the architectural implementation of the CNN model and its contribution to accomplishing these goals.

4.4. Performance Evaluation

The ultimate efficacy of the suggested CNN model was evaluated utilizing the independent testing set. Fig. 15 illustrates that the confusion matrix indicates the model attained exceptional classification accuracy across all three categories, with merely four misclassified samples out of 887. Table 4 elaborates on the evaluation measures, indicating a micro-accuracy of 99.78%, an average precision of 99.74%, an average recall of 99.77%, and a comprehensive F1-score of 99.75%. Per-class F1-scores were consistently elevated, attaining 99.67% for Benign, 100.00% for Cancer, and 99.61% for Normal. These findings validate the resilience of the proposed CNN architecture and the efficacy of the preprocessing pipeline in guaranteeing accurate categorization of mammography pictures.

This model's primary strength is its lightweight construction, enabling excellent precision alongside computing efficiency. The implementation of three convolutional blocks, accompanied by batch normalization and max pooling, facilitated the extraction of distinctive features while preventing overfitting, and the preprocessing processes markedly improved image quality. Notwithstanding these advantages, the model possesses specific constraints. The study was initially performed on the Mini-DDSM dataset, which,

despite its widespread utilization, may not adequately represent the heterogeneity of real-world mammography pictures across diverse populations and imaging modalities. Secondly, although the model attained near-perfect accuracy on the testing set, its generalizability to larger, more heterogeneous datasets requires validation.

The suggested approach exhibits competitive, and in certain instances superior, performance relative to prior work on mammography picture classification. Earlier studies utilizing conventional CNN architectures on the DDSM dataset indicated accuracies of 93% and 97%, whereas investigations applying more sophisticated deep learning models, such as ResNet or DenseNet, generally attained accuracies of 97% to 99%. This study's lightweight CNN achieved an accuracy of 99.78%, demonstrating that well-structured shallow architectures, when paired with efficient preprocessing, may compete with or exceed the performance of deeper, more resource-intensive models. These findings emphasize that the proposed CNN not only attains state-of-the-art performance but also provides a computationally efficient framework suitable for implementation in clinical assistance systems for early breast cancer identification.

4.5. Discussion

This study's results indicate that the suggested lightweight CNN architecture, in conjunction with a thorough preprocessing pipeline, can achieve near-perfect performance in categorizing mammography pictures into Normal, Benign, and Cancer categories. The model achieves an accuracy of 99.78% and consistently demonstrates elevated precision, recall, and F1-scores, confirming that critical diagnostic features, including microcalcifications and tissue patterns, are successfully recorded and assimilated. These findings underscore the significance of meticulously crafted preprocessing stages, which enhanced image quality and improved the CNN's capacity to extract discriminative features, despite its relatively superficial architecture.

The elevated classification performance suggests considerable promise for aiding radiologists in the early identification of breast cancer. By automating the classification of mammography images, the model can alleviate diagnostic workload, diminish human error, and furnish a dependable second opinion to enhance clinical decision-making. Timely and precise differentiation between benign and malignant abnormalities is essential for establishing suitable patient management strategies, hence enhancing survival rates and treatment results. Consequently, the proposed methodology emphasizes the role of deep learning as an auxiliary tool in contemporary medical imaging techniques.

Notwithstanding the encouraging outcomes, there remains room for improvement to advance further. The model was trained and evaluated using the Mini-DDSM dataset, which, despite being well-established, may not comprehensively reflect the diversity of clinical mammography data found in real-world scenarios. Subsequent research should encompass assessments on bigger and more diverse datasets to confirm generalizability. Moreover, incorporating sophisticated augmentation techniques, attention mechanisms, or transfer learning methodologies could significantly improve robustness and adaptability. Extending the paradigm to incorporate multi-modal imaging data, such as the integration of mammography with ultrasound or MRI, gives a promising opportunity to enhance diagnostic efficacy.

In conclusion, the discourse highlights that although the proposed CNN exhibits exceptional performance and significant utility in facilitating breast cancer screening, its overall influence will rely on ongoing enhancement, validation with real-world clinical data, and incorporation into current healthcare systems.

5. Conclusions

This study introduced a streamlined Convolutional Neural Network (CNN) model integrated with an extensive preprocessing pipeline for the categorization of mammography images. The preprocessing stages, comprising resizing, cropping, grayscale conversion, Laplacian of Gaussian (LoG) filtering, Gabor filtering, global threshold segmentation, and image sharpening, were effective in improving image quality and highlighting diagnostically pertinent features before model training.

The suggested CNN attained consistently superior performance, with a validation accuracy of 99.55% and a test accuracy of 99.78%. The findings were additionally corroborated by F1-scores surpassing 0.99 in all diagnostic categories (Normal, Benign, and Cancer). The results validate that the model can consistently identify essential characteristics, including microcalcifications and tissue architectures, hence guaranteeing strong classification efficacy. This result was achieved with a relatively shallow CNN comprising only three convolutional blocks, illustrating that a lightweight architecture, when combined with efficient preprocessing, can yield accuracy equivalent to or exceeding that of more intricate deep learning models.

The proposed technique highlights the capability of CNN-based systems to assist radiologists in the early diagnosis of breast cancer from a clinical standpoint. This approach enhances classification accuracy and minimizes diagnostic errors, so facilitating more dependable screening, prompt intervention, and ultimately better patient outcomes.

In contrast to previous studies that generally indicated accuracies between 93–97% for standard CNNs and 97–99% for more complex designs like ResNet and DenseNet, the current research demonstrated enhanced performance. This illustrates that computationally efficient models can achieve state-of-the-art outcomes, rendering them more appropriate for practical clinical applications where resources and time are frequently limited.

Subsequent research must confirm the generalizability of this methodology by implementing it on larger and more varied datasets that encompass various imaging circumstances and demographics. Further enhancements, including the integration of sophisticated augmentation strategies, transfer learning, or attention mechanisms, along with the expansion of the framework to multi-modal imaging—such as the combination of mammography with ultrasound or MRI—could enhance the robustness and clinical applicability of the system.

6. CRediT Authorship Contribution Statement

Abdul Latief Mufti: Data curation, Formal Analysis, Investigation, Project administration, Resources, Software, Visualization, Writing – original draft, and Writing – review & editing. **Adithya Kusuma Whardana:** Conceptualization, Investigation, Methodology, Project administration, Supervision, and Validation.

7. Declaration of Competing Interest

The authors declare that they have no known competing financial interests or personal relationships that could have appeared to influence the work reported in this paper.

8. Acknowledgments

We would like to express our gratitude to the reviewers for their precise and succinct recommendations that improved the presentation of the results obtained. Additionally, we extend our heartfelt thanks to Kaggle for providing the Mini-DDSM dataset, which played a crucial role in our research. The accessibility and quality of this open-source dataset have significantly contributed to the advancement of our study in early breast cancer detection.

9. Data Availability

The dataset used in this study, Mini-DDSM, is publicly available on Kaggle. Interested parties may access the dataset through the following link: https://www.kaggle.com/datasets/cheddad/miniddsm.

10. References

Alfayat, M. P., & Whardana, A. K. (2024). Deteksi Dini Alzheimer pada Otak dengan Kombinasi Metode. *Scan: Jurnal Teknologi Informasi dan Komunikasi, 19*(1), 32-41. doi:https://doi.org/10.33005/scan.v19i1.4735

Al-masni, M. A., Al-antari, M. A., Park, J. M., Gi, G., Kim, T. Y., Rivera, P., . . . Kim, T.-S. (2017). Detection and classification of the breast abnormalities in digital mammograms via regional Convolutional Neural Network. *2017 39th Annual International Conference of the IEEE Engineering in Medicine and Biology Society (EMBC). 39.* Jeju, Korea (South): IEEE. doi:https://doi.org/10.1109/EMBC.2017.8037053

American Cancer Society. (2014). *Cancer Facts & Figures 2014.* Atlanta, Georgia, United States: American Cancer Society. Retrieved from https://www.cancer.org/content/dam/cancer-org/research/cancer-facts-and-statistics/annual-cancer-facts-and-figures/2014/cancer-facts-and-figures-2014.pdf

Annisa, S., Lubis, Z., & Najmita, A. (2020). Perancangan Aplikasi Jaringan Syaraf Tiruan (Neural Networks) Untuk Pedeteksi Keaslian Uang Kertas. *JET (Journal of Electrical Technology), 5*(1), 1-8. Retrieved 9 23, 2025, from https://jurnal.uisu.ac.id/index.php/jet/article/view/2562

Basheer, N. M., & Mohammed, M. H. (2013). Segmentation of Breast Masses in Digital Mammograms Using Adaptive Median Filtering and Texture Analysis. *International Journal of Recent Technology and Engineering (IJRTE), 2*(1), 39-43. Retrieved 9 23, 2025, from https://www.researchgate.net/publication/326589085_Segmentation_of_Breast_Masses_in_Digital_Mammograms_Using_Adaptive_Median_Filtering_and_Texture_Analysis

Brahimetaj, R., Willekens, I., Massart, A., Forsyth, R., Cornelis, J., Mey, J. D., & Jansen, B. (2022). Improved automated early detection of breast cancer based on high resolution 3D micro-CT microcalcification images. *BMC Cancer, 22*. doi:https://doi.org/10.1186/s12885-021-09133-4

Brian, T. (2016). Analisis Learning Rates pada Algoritma Backpropagation untuk Klasifikasi Penyakit Diabetes. *Jurnal Ilmiah Edutic: Pendidikan dan Informatika, 3*(1), 21-27. doi:https://doi.org/10.21107/edutic.v3i1.2557

Cardona, H. D., Orozco, Á., & Álvarez, M. A. (2014). Automatic Recognition of Microcalcifications in Mammography Images through Fractal Texture Analysis. *ISVC: International Symposium on Visual Computing. 8888.* Las Vegas, NV, USA: Springer. doi:https://doi.org/10.1007/978-3-319-14364-4_81

Dyanti, G. A., & Suariyani, N. L. (2016). Faktor-Faktor Keterlambatan Penderita Kanker Payudara dalam Melakukan Pemeriksaan Awal ke Pelayanan Kesehatan. *KEMAS: Jurnal Kesehatan Masyarakat, 11*(2), 276-284. doi:https://doi.org/10.15294/kemas.v11i2.3742

Fadil, R., Jackson, A., Majd, B. A., Ghazi, H. E., & Kaabouch, N. (2019). Segmentation of Microcalcifications in Mammograms: A comparative Study. *2019 IEEE International Conference on Electro Information Technology (EIT).* Brookings, SD, USA: IEEE. doi:https://doi.org/10.1109/EIT.2019.8833735

Fuadi, I. H. (2023, 11 21). *4 Perbedaan AI, Machine Learning, dan Deep Learning + Contoh*. Retrieved 9 23, 2025, from Sanana Digital: https://sasanadigital.com/perbedaan-artificial-intelligence-machine-learning-dan-deep-learning-serta-contohnya/

Ghosal, S. K., Mandal, J. K., & Sarkar, R. (2018). High payload image steganography based on Laplacian of Gaussian (LoG) edge detector. *Multimedia Tools and Applications, 77*, 30403–30418. doi:https://doi.org/10.1007/s11042-018-6126-y

Gu, H., Wang, Y., Hong, S., & Gui, G. (2019). Blind Channel Identification Aided Generalized Automatic Modulation Recognition Based on Deep Learning. *IEEE Access, 7*, 110722-110729. doi:http://doi.org/10.1109/ACCESS.2019.2934354

Guo, Z., Xie, J., Wan, Y., Zhang, M., Qiao, L., Yu, J., . . . Yao, Y. (2022). A review of the current state of the computer-aided diagnosis (CAD) systems for breast cancer diagnosis. *Open Life Sciences, 17*(1), 1600-1611. doi:https://doi.org/10.1515/biol-2022-0517

Gupta, A., Anjum, A., Gupta, S., & Katarya, R. (2021). InstaCovNet-19: A deep learning classification model for the detection of COVID-19 patients using Chest X-ray. *Applied Soft Computing, 99*. doi:https://doi.org/10.1016/j.asoc.2020.106859

Guzmán-Cabrera, R., Guzmán-Sepúlveda, J. R., Torres-Cisneros, M., May-Arrioja, D. A., Ruiz-Pinales, J., Ibarra-Manzano, O. G., . . . Parada, A. G. (2013). Digital Image Processing Technique for Breast Cancer Detection. *International Journal of Thermophysics, 34*(8-9), 1519–1531. doi:https://doi.org/10.1007/s10765-012-1328-4

Houssein, E. H., Helmy, B. E.-d., Oliva, D., Elngar, A. A., & Shaban, H. (2021). Multi-level Thresholding Image Segmentation Based on Nature-Inspired Optimization Algorithms: A Comprehensive Review. In D. Oliva, E. H. Houssein, & S. Hinojosa, *Metaheuristics in Machine Learning: Theory and Applications* (Vol. 967). Springer. doi:https://doi.org/10.1007/978-3-030-70542-8_11

International Agency for Research. (2022). Indonesia. *GLOBOCAN 2022*. Retrieved 9 23, 2025, from https://gco.iarc.who.int/media/globocan/factsheets/populations/360-indonesia-fact-sheet.pdf

Iranmakani, S., Mortezazadeh, T., Sajadian, F., Ghaziani, M. F., Ghafari, A., Khezerloo, D., & Musa, A. E. (2020). A review of various modalities in breast imaging: technical aspects and clinical outcomes. *Egyptian Journal of Radiology and Nuclear Medicine, 51*. doi:https://doi.org/10.1186/s43055-020-00175-5

Iriyanto, S. Y., & Zaini, T. M. (2014). *Pengolahan Citra Digital.* Bandar Lampung, Indonesia: Anugrah Utama Raharja (AURA).

Jothiaruna, N., Sundar, K. J., & Ahmed, M. I. (2021). A disease spot segmentation method using comprehensive color feature with multi-resolution channel and region growing. *Multimedia Tools and Applications, 80*, 3327–3335. doi:https://doi.org/10.1007/s11042-020-09882-7

Kadir, A., Nugroho, L. E., Susanto, A., & Santosa, P. I. (2011). Foliage Plant Retrieval Using Polar Fourier Transform, Color Moments and Vein Features. *Signal & Image Processing : An International Journal (SIPIJ), 2*(3). doi:http://doi.org/10.5121/sipij.2011.2301

Kamil, M. Y. (2020). Computer-aided diagnosis system for breast cancer based on the Gabor filter technique. *International Journal of Electrical and Computer Engineering, 10*(5), 5235-5242. doi:http://doi.org/10.11591/ijece.v10i5.pp5235-5242

Khan, A., & Arora, A. S. (2019). Breast Cancer Detection Through Gabor Filter Based Texture Features Using Thermograms Images. *2018 First International Conference on Secure Cyber Computing and Communication (ICSCCC). 1.* Jalandhar, India: IEEE. doi:https://doi.org/10.1109/ICSCCC.2018.8703342

Khoulqi, I., & Idrissi, N. (2020). Segmentation and Classification of Microcalcifications Using Digital Mammograms. *The Proceedings of the 4th International Conference on Smart City Applications. 4*, pp. 384–403. Casablanca, Morocco: Springer. doi:https://doi.org/10.1007/978-3-030-37629-1_29

Leong, Y. S., Hasikin, K., Lai, K. W., Zain, N. M., & Azizan, M. M. (2022). Microcalcification Discrimination in Mammography Using Deep Convolutional Neural Network: Towards Rapid and Early Breast Cancer Diagnosis. *Frontiers in Public Health, 10*. doi:https://www.frontiersin.org/journals/public-health/articles/10.3389/fpubh.2022.875305/full

Liew, X. Y., Hameed, N., & Clos, J. (2021). A Review of Computer-Aided Expert Systems for Breast Cancer Diagnosis. *Cancers, 13*(11). doi:https://doi.org/10.3390/cancers13112764

Logullo, A. F., Prigenzi, K. C., Nimir, C. C., Franco, A. F., & Campos, M. S. (2022). Breast microcalcifications: Past, present and future (Review). *Molecular and Clinical Oncology, 16*(4). doi:https://doi.org/10.3892/mco.2022.2514

Madhavi, M. V., & Bobby, T. C. (2019). Gabor Filter Based Classification of Mammography Images Using LS-SVM and Random Forest Classifier. *Recent Trends in Image Processing and Pattern Recognition Second International Conference, RTIP2R 2018. 1036*, pp. 69–83. Solapur, India: Springer. doi:https://doi.org/10.1007/978-981-13-9184-2_6

Mohimont, L., Alin, F., Rondeau, M., Gaveau, N., & Steffenel, L. A. (2022). Computer Vision and Deep Learning for Precision Viticulture. *Agronomy, 12*(10). doi:https://doi.org/10.3390/agronomy12102463

Moyya, P. D., & Asaithambi, M. (2022). Quantitative Analysis of Breast Cancer NACT Response on DCE-MRI Using Gabor Filter Derived Radiomic Features. *International Journal of Online and Biomedical Engineering, 18*(12), 106–122. doi:http://doi.org/10.3991/ijoe.v18i12.32501

Nagane, U. P., & Mulani, A. O. (2021). Moving Object Detection and Tracking Using Matlab. *Journal of Science & Technology, 6*(Special Issue 1), 63–66. Retrieved 9 23, 2025, from https://jst.org.in/index.php/pub/article/view/743

Narasimhaiah, P., & Nagaraju, C. (2023). Breast Cancer Screening Tool Using Gabor Filter-Based Ensemble Machine Learning Algorithms. *International Journal of Intelligent Systems and Applications in Engineering, 11*(2), 936–947. Retrieved 9 23, 2025, from https://ijisae.org/index.php/IJISAE/article/view/2972

Podgornova, Y. A., & Sadykov, S. S. (2019). Comparative analysis of segmentation algorithms for the allocation of microcalcifications on mammograms. *International Conference on "Information Technology and Nanotechnology" (ITNT-2019). V.* Samara, Russia: CEUR-WS.org. Retrieved 9 23, 2025, from https://ceur-ws.org/Vol-2391/paper17.pdf

Saifullah, S., Sunardi, S., & Yudhana, A. (2016). Analisis Perbandingan Pengolahan Citra Asli Dan Hasil Croping Untuk Identifikasi Telur. *JuTISI (Jurnal Teknik Informatika dan Sistem Informasi) (e-Journal), 2*(3), 341-350. Retrieved 9 23, 2025, from https://journal.maranatha.edu/index.php/jutisi/article/view/638

Salama, W. M., & Aly, M. H. (2021). Deep learning in mammography images segmentation and classification: Automated CNN approach. *Alexandria Engineering Journal, 60*(5), 4701-4709. doi:https://doi.org/10.1016/j.aej.2021.03.048

Sama, A. S., & Baneamoon, S. M. (2017). Breast Cancer Classification Enhancement Based on Entropy Method. *International Journal of Engineering and Applied Computer Science (IJEACS), 2*(8), 267-271. doi:http://doi.org/10.24032/ijeacs/0208/06

Sarker, I. H. (2021). Machine Learning: Algorithms, Real-World Applications and Research Directions. *SN Computer Science, 2*(3). doi:https://doi.org/10.1007/s42979-021-00592-x

Singh, A. K., & Gupta, B. (2015). A Novel Approach for Breast Cancer Detection and Segmentation in a Mammogram. *Procedia Computer Science, 54*, 676-682. doi:https://doi.org/10.1016/j.procs.2015.06.079

Singh, G., & Goel, A. K. (2020). Face Detection and Recognition System using Digital Image Processing. *2020 2nd International Conference on Innovative Mechanisms for Industry Applications (ICIMIA). 2.* Bangalore, India: IEEE. doi:https://doi.org/10.1109/ICIMIA48430.2020.9074838

Wang, K., Ye, Z., Xie, X., Cui, H., Chen, T., & Liu, B. (2024). MLN-net: A multi-source medical image seg-

mentation method for clustered microcalcifications using multiple layer normalization. *Knowledge-Based Systems, 283*. doi:https://doi.org/10.1016/j.knosys.2023.111127

Whardana, A. K., & Putri, R. K. (2025). Comparative Evaluation of Supervised Learning Algorithms for Breast Cancer Classification. *International Journal of Engineering and Manufacturing (IJEM), 15*(4), 29-38. doi:https://doi.org/10.5815/ijem.2025.04.03

Whardana, A. K., Mufti, A. L., Hermawan, H., & Aziz, U. A. (2024). Classification Techniques in Finding Malignant Breast Cancer Detection. *Journal of Information Technology and Cyber Security, 2*(1), 40–50. doi:https://doi.org/10.30996/jitcs.8829

World Health Organization. (2022, February 4). *Urgently address gaps in cancer care: WHO*. Retrieved 9 23, 2025, from World Health Organization: https://www.who.int/southeastasia/news/detail/04-02-2022-urgently-address-gaps-in-cancer-care-who#:~:text=New%20Delhi%20%7C%204%20February%202022,people%20suffering%20from%20the%20disease.

Zamir, R., Bagon, S., Samocha, D., Yagil, Y., Basri, R., Sklair-Levy, M., & Galun, M. (2021). Segmenting microcalcifications in mammograms and its applications. *Medical Imaging 2021: Image Processing. 11596*, pp. 788-795. SPIE. doi:https://doi.org/10.1117/12.2580398

Zhang, C., & Lu, Y. (2021). Study on artificial intelligence: The state of the art and future prospects. *Journal of Industrial Information Integration, 23*. doi:https://doi.org/10.1016/j.jii.2021.100224

Zhao, J., Chen, T., & Cai, B. (2022). A computer-aided diagnostic system for mammograms based on YOLOv3. *Multimedia Tools and Applications, 81*(14), 19257–19281. doi:https://doi.org/10.1007/s11042-021-10505-y